MNE 16 (2022) 100159

Contents lists available at ScienceDirect

Micro and Nano Engineering

journal homepage: www.sciencedirect.com/journal/micro-and-nano-engineering

Combined masked LCD-printing and microfabrication for bioimpedance-chips

Julia Linert [a,b,1], Philipp Taus [a,1], Sonia Prado-López [a], Markus Pribyl [a], Samuele M. Dozio [a], Michael J. Haslinger [c], Elena Guillen [c], Michael Muehlberger [c], Heinz D. Wanzenboeck [a,*]

[a] TU Wien, Institute of Solid State Electronics, Vienna A-1040, Austria
[b] TU Wien, Institute of Applied Physics, Vienna A-1040, Austria
[c] PROFACTOR GmbH, Steyr 4407, Austria

ARTICLE INFO

Keywords:
Microfluidic device
3D printing
On-Chip printing
Biocompatibility

ABSTRACT

Biomedical in vitro sensors use cell cultures grown on sensor chips for drug testing, toxicological screening, studying pathologic processes in tissue and for personalized medicine. Microfluidic systems and chips bridge the gap of the biological micro world to our accessible macro world, creating the interface between e.g., cells on a chip to reservoirs and pumps. Prototype and low volume lab scale microfluidic devices have traditionally been realized by soft lithography using polydimethylsiloxane (PDMS) technology. Recently, rapid prototyping of microfluidic devices using direct 3D printing has become widely available. Usually, the 3D printed parts are (i) either stand-alone systems requiring only fluidic connections, or (ii) they need to be carefully aligned and skilfully attached to the rigid micro fabricated chip. This post-fabrication attachment is time-consuming and a frequent source of error. In this work the fabrication of the microchip and the microfluidic system have been integrated into a multi technology fabrication process. For the first time we demonstrate the "on-chip 3D printing" of a microfluidic attachment directly onto an in-house fabricated multi electrode array chip. The process uses a desktop-sized LCD resin printer and eliminates the time-consuming post-deposition alignment and attachment. Biocompatibility of the used resin was confirmed for murine fibroblasts and validates this multi technology approach for biomedical cell chips.

1. Introduction

Microfluidic systems are essential for many biomedical in-vitro devices, including lab-on-a-chip-devices, drug testing or disease modelling [1,2]. To form such a device, often, two functional entities can be identified: (a) a (micro-)fluidic compartment and (b) a separate sensor substrate, such as a microchip. There are several manufacturing approaches that allow constructing the fluidic unit with varying degrees of resolution and 3D capability (Fig. 1). For further information see supporting information Table S1.

One standard approach is polydimethylsiloxane (PDMS) based soft-lithography [3] using epoxy SU-8 master moulds or 2-photon-polymerization printed templates [4]. This method allows for high resolution imprints, but comparatively poor aspect ratios and limited 3D capability in single- and few layer processes. Moreover, this requires thin-film equipment and process development. Recent advances in laser pyrolysis allow for digital patterning of PDMS [5] and Polyimide [6] of 2D and quasi 3D structures.

Another manufacturing technique that has recently gained attention is direct 3D printing of microfluidic components [7–9]. Especially LCD resin printers have gained increasing popularity as they offer a cost-efficient possibility of fast design adaption and prototyping of 3D structures. While the printing resolution is still inferior to photolithography, microfluidic structures of several centimetres height can be fabricated in a single step. Furthermore, biocompatibility, low optical transparency, high surface roughness and low gas permeability are notable challenges [10,11]. Another 3D printing technology, namely 2-photon-polymerization is also very popular method, since very small features with submicron dimensions can be printed without the need of supporting structures [12]. However, this technology is still very expensive and requires intensive testing and process optimisation.

A major problem for the fabrication of microfluidic devices is the

* Corresponding author.
E-mail address: heinz.wanzenboeck@tuwien.ac.at (H.D. Wanzenboeck).
[1] These authors contributed equally.

https://doi.org/10.1016/j.mne.2022.100159
Received 13 December 2021; Received in revised form 31 May 2022; Accepted 10 July 2022
Available online 14 July 2022

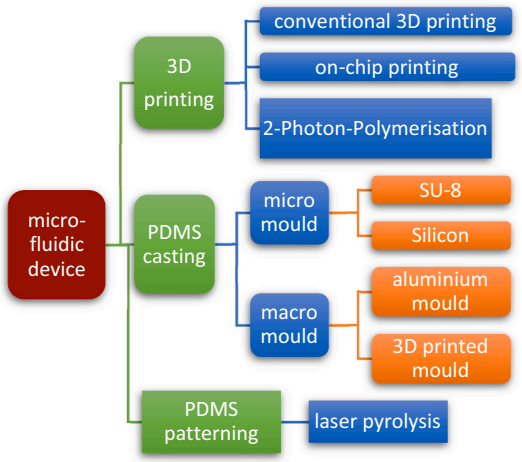

Fig. 1. Commonly used lab-scale fabrication approaches of microfluidic devices as well as the proposed method.

precise attachment of the cell compartment to electrical active sensor surfaces [13]. In the case of multi electrode arrays (MEAs) used for electrophysiological recordings, usually a simple well is glued or bonded [14–17] onto the electrically active substrate that was processed by conventional lithography. The accurate attachment of a top unit featuring delicate channels requires a lot of attention and manual dexterity. Inaccurate placement is a frequent source of biochip malfunction and leakage. To overcome this bottleneck, it would be beneficial to avoid the conventional two-step fabrication and combine photolithography and 3D printing in a single process.

In this work, we demonstrate a combined micro- and macro technology masked LCD printing with photolithographic microfabrication. The top unit with a simple design has three main components: an inlet, a channel and an outlet. Cells can be placed in the system and moved to the desired position. The is top unit is 3D printed onto a micro structured MEA substrate (Fig. 2). To our knowledge, no on-chip 3D printing process was described in literature so far.

2. Materials & methods

In the following section, the fabrication of the different parts of an exemplary microfluidic biochip, as shown in Fig. 2 is described.

2.1. Fabrication of the microelectrode Array (MEA) sensor substrate

Multi electrode array substrates were fabricated using conventional i-line photolithography, metal and insulator deposition techniques and

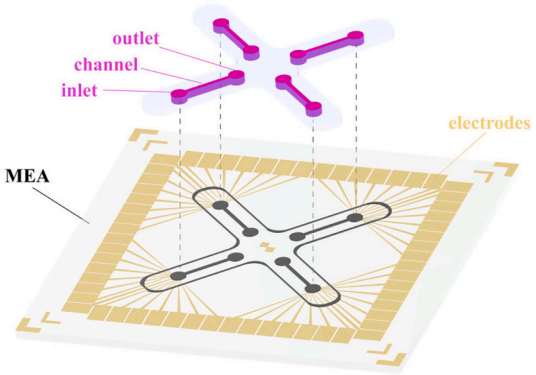

Fig. 2. Exploded view of the microfluidic compartment (top) and the microelectrode array (MEA). MEA size: 49 × 49 mm.

reactive ion etching (Fig. S1). First, the bare 49 × 49 mm glass substrates (D263TEco, Schott, Malaysia) were cleaned in acetone and isopropyl alcohol and dried under a stream of nitrogen. A subsequent dehydration bake at 120 °C was performed to remove residual moisture. The surface was then pre-treated using an adhesion promoter (TI-prime, micro resist technology, Germany). The AZ 5214E photo resist (Microchemicals GmbH, Germany) was processed in image reversal mode according to the manufacturer's instructions using a MJB3 mask aligner (SÜSS MicroTec SE, Germany). A Titanium (10 nm) and Gold (300 nm) stack was sputter deposited (Von Ardenne LS 320 S, Germany) and subsequently lifted-off in an acetone bath. The substrate was then passivated by a plasma enhanced chemical vapour deposition process (Plasmalab 80 plus, Oxford Instruments, UK) with silicon nitride (Si_3N_4, 300 nm). A second lithography step defined the openings in the passivation layer where the measuring electrodes are exposed. To remove the passivation, an SF_6 based reactive ion etching process was performed using a Plasmalab 100 (Oxford Instruments, UK) tool. Final cleaning of the substrate was carried out in an ultrasonic bath using acetone and isopropyl alcohol.

2.2. Microfluidic compartment

2.2.1. Conventional 3D printing and post processing

3D prints were fabricated using masked-LCD printers (Photon Mono X, Anycubic Technology, Hongkong and Phrozen Sonic Mini 4 K, Phrozen Technology, Taiwan) with a 405 nm UV light source. Commercially available resin (AOE-CMR-BASIC, niceshops GmbH, Austria) was used as photo-hardening (negative tone) polymer.

A CAD (computer aided-design) model (Fig. 2) was generated and subsequently processed into a printer-readable file format using the slicing software Chitubox v1.8.1 (Chitubox, China) and pre-set parameters. Before each print, the build plate was accurately levelled according to the manufacturer's instructions. After completion of the 3D print, the build plate was suspended at a 45° tilt angle to facilitate uncured resin drip off. Subsequently, the 3D prints were carefully detached from the build plate, cleaned in an ultrasonic bath using clean isopropyl alcohol and dried under a stream of nitrogen. Parts were then post-cured with UV light (405 nm) using the Anycubic Wash and Cure Station (Anycubic Technology, Hongkong) for five minutes. To ensure full curing, parts were optionally thermally post-cured [18].

For the biocompatibility assessment, thin cover slips (thickness: 300 µm, diameter: 10 mm) were 3D printed according to the aforementioned process. The cured resin was subsequently used as substrate for growth of murine fibroblasts (see 2.3).

2.2.2. On-Chip 3D printing

For on-chip printing the procedure as described above was conducted directly on microelectrode arrays on glass substrates fabricated as described in 2.1. For 3D printing on the MEAs the following adaptations were implemented:

2.2.2.1. Attachment and positioning. Before 3D printing of the microfluidic system the MEA had to be mounted on the build plate using three different methods. (a) Adhesive spray (3 M, Austria) was applied from a distance of 50 cm using a cut-out stencil to cover the rest of the build plate. The substrate was then brought in contact manually and UV irradiated to facilitate hardening of the adhesive. (b) Thin tape was applied on the edges of the substrate, wrapping around the build plate. (a) and (b) used a stencil to centre the substrate with respect to the printed microfluidic compartment. (c) A customised 3D printed vacuum chuck (Fig. S2) was used as build plate substitute, which also provided centred positioning to the LCD screen.

2.2.2.2. Adhesion promotion. TI-prime (Microchemicals GmbH, Germany) and permanent epoxy negative photoresist SU-82015

(Microchem, USA) were spin-coated (nominal height: 21 μm) onto the glass substrate or MEA and processed according to the manufacturer's instructions using a MJB3 mask aligner (SÜSS MicroTec SE, Germany). The substrate with pre-patterned SU-8 was then attached to the build plate using the aforementioned methods and the 3D printing process was started. Post-treatment steps were the same as for conventional 3D printing.

2.2.3. Characterization

The surface of the finished 3D prints as well as cell coatings on the 3D printed substrates were characterized by microscopy. Bright-field and fluorescence microscopy were performed using an inverted microscope (Eclipse TE200, Nikon, Japan) with a Hamamatsu Digital CMOS Camera (C13440-20CU, Hamamatsu Photonics K.K., Japan). Scanning electron microscopy (SEM) (CrossBeam Neon40XB, Zeiss, Austria) was performed after sputter coating of a 20 nm gold layer, to assess alignment and print quality after post-processing. In order to characterise the surface roughness of the 3D printed parts, a stylus profilometer (DektakXT, Bruker, USA) was used.

Leak-tight operation was assessed by dispersing coloured, aqueous liquids into the designated inlet cavities and by visual comparison after an incubation time of one hour.

2.3. Biocompatibility assessment

2.3.1. Cell culturing

The murine fibroblast cell line BALB/3 T3 clone A31 (Lonza, Italy) was employed to check the possible effects of the 3D printing resin on cellular viability. The cells were detached from culture flasks using accutase (Sigma Aldrich, Austria) and subsequently centrifuged. Cell number and viability were assessed with trypan blue dye exclusion test. 3D printed cover slips and standard plastic cover slips for control were sterilized with two washes of ethanol at 75%. Each sample was seeded by dropping 20 μl of cell suspension (20.0×10^4 cells) on top, allowing cell attachment before adding the cell culture medium in a 24 well plate. The cells were cultured for 48 h under an atmosphere containing 5% CO_2 at 37 °C in a standard medium consisting of Dulbecco's Modified Eagle's Medium (Lonza, USA), 10% bovine calf serum (Sigma Aldrich, Vienna, Austria) and penicillin-streptomycin (100 Units/ml, 100 μg/ml) (Lonza, USA). All cell handling procedures were performed in a sterile laminar flow hood.

2.3.2. Proliferation assay

Quantitative viability test was performed via Cell Counting Kit-8 (CCK-8) (MedChemExpress LLC, USA) assay. At each time point (1, 2, and 3 days) the solution of CCK-8 was added in proportion 1:10 to the 3D printed samples and controls. After two hours of incubation at 37 °C and 5% CO_2, the supernatant was transferred to a 96-well plate and the absorbance was read at 450 nm using an Enzo Absorbance 96 Plate Reader (Enzo Life Sciences, Inc., USA). The measured absorbance is directly proportional to the number of metabolically active cells. For each time point, nine samples were evaluated.

2.3.3. Cell viability assay

After 48 h in culture, the cells on the 3D printed samples and the control were stained with Hoechst 33342 and Propidium iodide (PI). Cell staining was visualized using the inverted fluorescence microscope.

2.4. Bioimpedance measurement

2.4.1. Measurement setup

The on-chip printed device was filled with fibroblast growth medium (Sigma-Aldrich) and the measurement setup (Sciospec ISX-3) internal calibration routine was performed. Measurements were conducted within a frequency range of 1 Hz - 1 MHz at 20 points in logarithmic spacing. The measurement amplitude was set to 125 mV at the precision setting "0", with an average setting of "3". The spheroid was then loaded into the measurement chamber with a 300 μl pipette tip, and the measurement routine was run with the same settings as above. The measured spectra consist of the real and imaginary parts at the specific frequencies. Impedance magnitude $|Z|$ was calculated as the square root of the sum of the squares of real and imaginary part. The reference measurement $|Z_0|$ was used to calculate the percent change $|Z|/|Z_0|*100$.

2.4.2. Cell culturing for bioimpedance

Human dermal fibroblasts (HDF) (Merck) were cultured under an atmosphere containing 5% CO_2 at 37 °C in fibroblast growth medium (Sigma-Aldrich). Once confluent, the cells were raised with Accutase StemProTM (ThermoFisher). Next, the cells were seeded for spheroid formation in 12 well plates (Thermo Scientific Nunclon Sphera) at a density of 40.000 cells per well and cultivated for two weeks on spheroids induction media, consisting of 1:1 Ham's F12/ DMEM supplemented with 20 ng/ml de EGF, 10 ng/ml de bFGF, 5 μg/ml insulin and penicillin/streptomycin (Lonza, USA), at a working concentration of 100 units of potassium penicillin and 100 μg of streptomycin sulfate per 1 ml of culture media. Media was changed every second day and spheroids formation was monitored under the microscope.

3. Results & discussion

This work evaluates a multi technology approach that integrates 3D printing directly on a micro-structured sensor chip. Providing the liquid cell medium via a microfluidic system involves specific challenges for 3D printing:

3.1. Attachment and positioning

For the combination of micro- and macro-technologies to a multi-technology device the main problems are the attachment and the precise alignment. We investigated several methods as described in section 2.2: attachment and positioning.

Using adhesive spray to mount the glass substrate to the build plate led to movement of the substrate during printing. Subsequent detachment and cleaning proved to be difficult. When employing thin tape instead of the adhesive spray similar problems were observed. The most sophisticated, precise and reliable method was using the customised vacuum chuck (Fig. S2). In contrast to the other aforementioned gluing methods, the vacuum chuck has several advantages: (i) a more rigid fixation, leading to less substrate displacement during the printing process. This displacement is a potential source of severe print distortions as shown in Fig. S3. (ii) intrinsic sub-mm positioning of the substrate with regard to the LCD screen (iii) handling and cleaning workflow is significantly shorter (iv) easy detachment by breaking the vacuum.

3.2. Minimal channel size

Single human as well as murine fibroblast cells are in the range of 10–15 μm. Microfluidic designs for cell recordings feature structures of several 100 μm. To investigate the resolution limits of masked LCD printing, simple models of channels and holes of a size range of 50 μm to 2 mm were printed with varying exposure times in combination with a layer thickness of 25 μm on pristine glass substrates. The achievable minimal structure size depends on the exposure time, printer and used resin. For the combination of AOE-CMR-BASIC resin with the Phrozen Sonic Mini 4 K printer, an exposure time of 5 s was found to be optimal regarding minimum channel printability on a glass substrate (Fig. S4). Prints with shorter exposure time showed cracks and insufficient interlayer adhesion (tested with 3.5 s and 4 s). Longer exposure times lead to closed channels as a result of overexposure. To ensure proper curing of the bottom interface layers, the first four bottom layers were exposed for 20 s. This results in enlarged patterns due to light bleeding into

neighbouring pixels. An optical pattern correction value of −75 µm (expansion of cavities) for the four bottom layers was applied in order to compensate for overexposure effects. Our printed samples revealed that channels from a nominal size of 100 µm are printable and liquid flow is possible (Fig. S5 left). However, liquid-electrode contact can only be established for channels with a size of at least 200 µm (Fig. S5 right), where the bottom optical pattern correction is sufficient to prevent closure of the channels at the bottom layers. Generally, the error in channel width was within two pixels of the LCD screen, which in the case of the Phrozen Sonic Mini 4 K is 70 µm. In our design, we have chosen to keep the print optically transparent, in order to facilitate microscopic observation of the channels. Therefore, transparent resin was used, however we expect higher resolution results could be achieved with non-transparent resin, which limits light penetration depth.

3.3. On-Chip 3D printing

Current methods for microfluidic attachments onto high resolution photolithographically produced substrates are either limited in height (SU-8/PDMS) or prohibitively complex and expensive (2-photon-polymerization). To our knowledge there is no technology that allows research labs to produce 3D millimetre sized attachments for high resolution multi-electrode arrays. Especially 3D cell cultures in the form of spheroids need millimetre and sub-millimetre structures that facilitate nutrient supply and handling, so the sophisticated MEA technology can be fully utilized. To avoid a post-printing assembly step, the microfluidic structures have been directly deposited on a microelectrode array. Initial prints showed insufficient adherence and liquid leakage after post-curing with UV light. A lithographically patterned SU-8 layer was used as an intermediate adhesion layer, as well as a biocompatible encapsulation of the MEA. Fig. 3 (a) displays the successfully printed cell compartment on a microelectrode array. The visible 60 gold traces route the thin film gold electrodes (25 × 25 µm) to the outside of the chip to the respective contacting pads (2.2 × 3.5 mm) that are compatible for pogo-pin connection to a commercial electrophysiology measurement setup. The 3D printed attachment is based on the minimum channel size design (500 µm width, 6.5 mm length, inlet and outlet radii 1 mm). Tests with coloured, aqueous liquid showed that the channels are not leaking. The added i-line lithography (365 nm) step due to the SU-8 adhesion layer coating was necessary, because SU-8 shows reduced sensitivity to the Phrozen Sonic Mini 4 K's 405 nm illumination source. Using existing 405 nm sensitive photopolymers, similar to SU-8, this layer could potentially replace the underlying silicon nitride insulation. To further simplify the fabrication process, the adhesion layer could then directly be structured during printing.

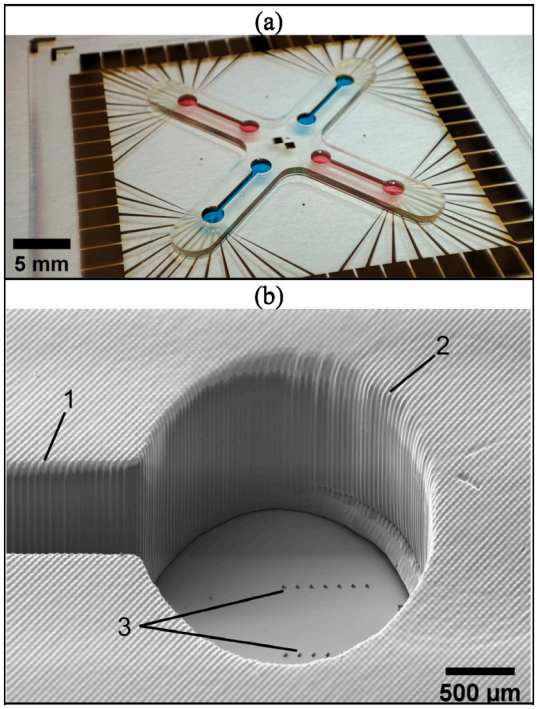

Fig. 3. Open microfluidic channel directly printed on a MEA chip with four separate channels.
(a) photograph of on-chip print showing the channels filled with coloured liquid
(b) 45° tilted SEM image, showing the electrical contacts of the MEA inside the 3D printed opening. (1) channel (2) measurement chamber (3) gold electrodes. (For interpretation of the references to colour in this figure legend, the reader is referred to the web version of this article.)

The 45° tilted SEM view in Fig. 3 (b) shows a detailed image of the same structure as in (a). Here the lithographically patterned gold microelectrodes are visible. The 25 µm wide gold trace is completely covered by SU-8 except for the lithographically defined 50 × 25 µm openings, forming 25 × 25 µm gold microelectrodes. All measurement and reference electrodes are open and not obstructed by resin residues or overexposure artefacts. There is a step visible at the transition of the four 20 s exposed bottom layers to the rest of the 5 s exposure normal layers, where the selected bottom layer correction of 75 µm was insufficient to fully compensate for the overexposure effect. Also, the whole print is shifted in the y- direction of the LCD matrix. This y-shift was caused by tolerance in the vacuum chuck fixation mechanism that is used for levelling. This could be improved in future revisions of the mounting mechanism. Fig. 3 (b) also reveals the individual pixels of the LCD matrix used to generate the vertical sidewalls of the 3D print. One possibility to alleviate this, is to use the printer's anti-aliasing setting, where several pixels are grey-value interpolated to generate a smooth contour. This however leads to broadening of structures. Therefore, the setting was disabled for optimal structure fidelity. A more detailed discussion of the surface roughness is given in 3.4.

After demonstrating feasibility of small, leak-tight and well-defined channels on glass substrates and multielectrode arrays, a multi-technology device with a conical inlet shown in Fig. 4, was fabricated. Biological samples can be examined in four identical microfluidic compartments (inlet, channel, outlet) for independent parallel real-time measurements.

The combination of micrometre-sized electrodes obtained by photolithography and the millimetre sized 3D printed cell compartment, allows for spatially resolved measurements with sufficient medium perfusion and nutrient supply to avoid drying out.

3.4. Bioimpedance measurements

In order to demonstrate the functionality of a finalized device, the

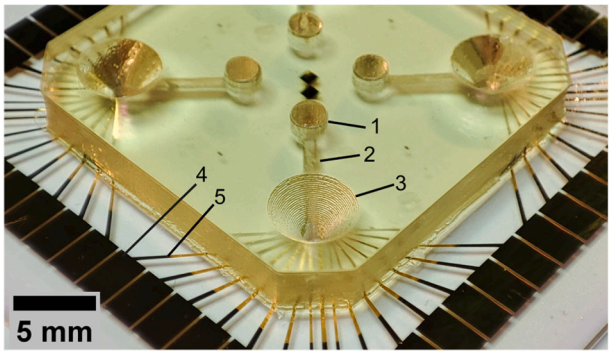

Fig. 4. Final device fabricated by multi-technology approach, to be used for electrophysiology measurements, featuring four inlet ports with channels and outlet ports.

design shown in Fig. 3 was used for bioimpedance sensing of cell spheroids. Fig. 5 shows the recorded impedance spectra with fibroblast medium (grey) and in presence of a spheroid (red and blue). The spheroid was positioned over one of the measurement microelectrodes, while another measurement electrode was selected as the counter (Fig. S7). A distinct difference in the recorded spectra is evident in presence of the spheroid, in the form of increased impedance in lower frequencies and decreased impedance at higher frequencies. The difference is stable over the spheroid observation time of 5 min.

3.5. Surface roughness

The flat surface of a conventional 3D print (surface facing the vat with a FEP (Fluorinated Ethylene Propylene Polymer) foil and an on-glass printed sample that was peeled off the glass substrate (surface facing the glass substrate) were examined with a profilometer. The assessed peak-to-peak surface roughness yielded 4 µm for the conventional 3D print and 8 nm for the on-glass print (Fig. S6). While normally not accessible to the environment, in our use case, the on-glass print displays enhanced optical properties, especially useful if transparency is required.

3.6. Biocompatibility and viability

For an application as in-vitro sensor the biocompatibility of the 3D printed microfluidic system is essential. To exclude cytotoxic effects and to confirm a good cell viability we investigated the biocompatibility with mice fibroblasts. Material samples of printed and post UV radiated AOE-CMR-BASIC resin were placed in a multiwell plate and used as substrate for the growth of cells over a duration of three days. The 3D printed cover slips with seeded mice fibroblasts (BALB/3 T3) were examined with bright field microscopy, Hoechst staining and Propidium iodide staining (see Fig. 6).

While Hoechst staining (blue) is a fluorescent dye that binds to the DNA of cells, highlighting their position, Propidium iodide (red) penetrates only dead cells. The surface roughness of the 3D printed sample can be seen in Fig. 6 (a). After 24 h a dense cell layer was observed

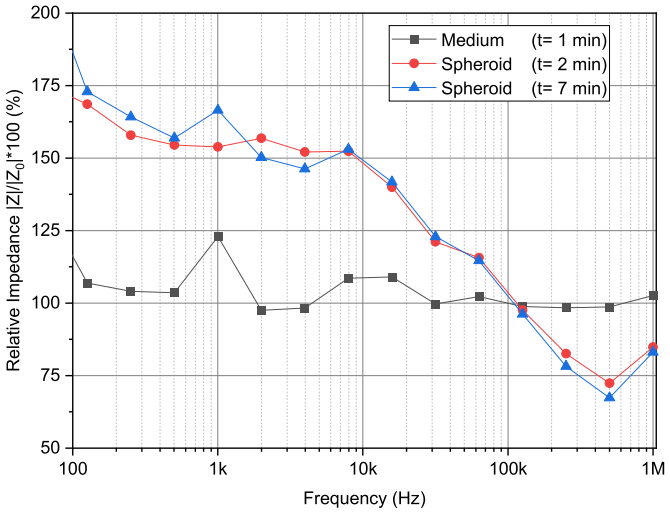

Fig. 5. Measured impedance spectra without (grey) and with a spheroid present (red and blue) over the measurement electrode. Impedance changes are computed with respect to reference measurement Z_0 at $t = 0$ with only cell medium and displayed from 100 Hz to 1 MHz. The grey line (1 min after reference measurement) shows only minimal deviation from the reference (100% line). The changes across the spectrum in the blue and red trace both indicate the presence of the spheroid. (For interpretation of the references to colour in this figure legend, the reader is referred to the web version of this article.)

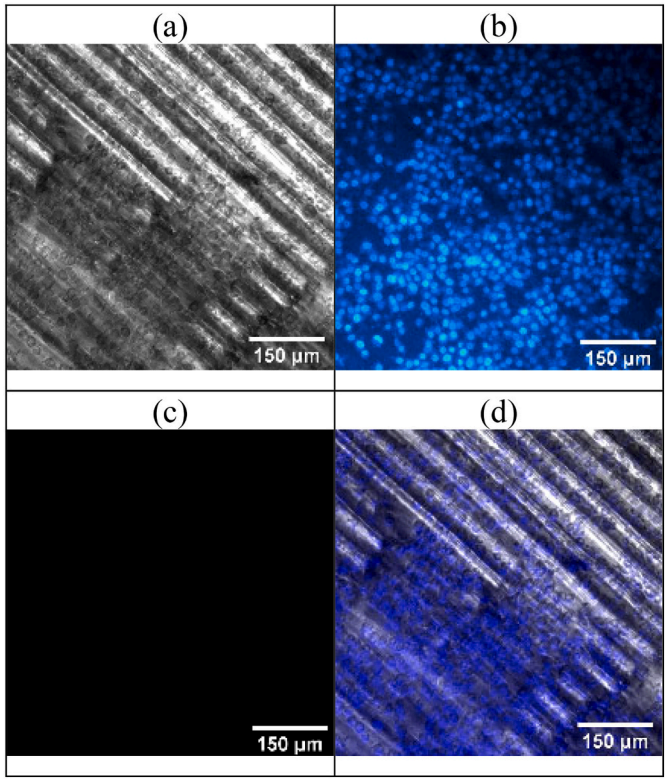

Fig. 6. (a) Bright-field microscope image of BALB/3 T3 mice fibroblast cells seeded on a 3D printed cover slip. (b) Hoechst staining of the sample, blue fluorescence is corresponding to the position of cells. (c) Propidium iodide staining of the sample, red fluorescence would correspond to dead cells (i.e., none detected). (d) Merged image of (a), (b) and (c)

(Fig. 6 (b)) by Hoechst staining and no dead cells were detected (Fig. 6 (c)) by Propidium iodide staining.

To ensure biocompatibility of the proposed 3D resin, i.e., to exclude any cytotoxic effect, the quantitative viability of the BALB/3 T3 cells was investigated. The CCK-8 assay yielded increasing absorbance over time, directly corresponding to the amount of metabolically active cells (Fig. 7). A highly statistical significance with $P < 0{,}0001$ was observed. According to our results of the biocompatibility assay, the BALB/3 T3 mice fibroblasts are capable to grow on the printed resin for at least 72 h and viability is not impaired. However, the proliferation capacity appears to be affected, especially at day three, if compared with the control

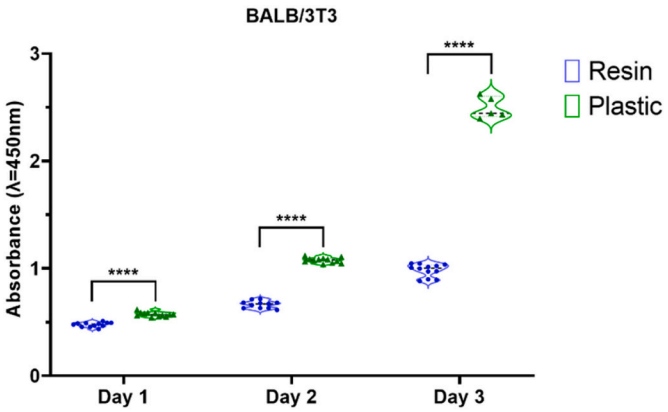

Fig. 7. CCK-8 cellular viability assay of mice fibroblast (BALB/3 T3 clone A31) cell line seeded on 3D printed cover slips and plastic cover slips (control) at 1, 2 and 3 days after seeding ($N^\circ = 9$). ****$P < 0{,}0001$.

on plastic (Fig. 7).

The 3D resin exhibited a slower doubling time compared to tissue culture plates. Due to the absence of apoptotic cells, which is confirmed by no detectable red fluorescence signal in the PI channel, the material can still be argued as biocompatible for short time cell cultures.

Biological investigations on how the resin might affect the division capacity of BALB/3 T3 cells [19–23], are in progress and will be published in a more biology-based publication.

4. Conclusion

The presented on-chip printing explores a way of combining micrometre scaled electronically active substrates produced by photolithography with rapid prototyping produced cell compartments in large millimetre scale. This method allows for combining alignment, attachment and interfacing to tubing systems into one step, opening new manufacturing possibilities that may be interesting for commercial serial production. The applicability of the proposed method was demonstrated by bioimpedance measurements of human fibroblast spheroids, as well as biocompatibility assessment of the used material. The used equipment for the realization of the microfluidic compartment is easily affordable and allows in combination with commercially available MEAs, an easy entry to biomedical microfluidic devices. The adaptable print platform allows for various printers to be used, however structural optimization and further machine modifications might significantly improve alignment accuracy. Another area for handling improvements is post-printing cleaning, which at the moment requires careful manual handling of the substrates. So far, the designs have been gravity driven or used with slight negative pressure. Whether the adhesion of the print requires further improvements for positive pressure closed systems remains to be seen and was not tested in this work.

Funding

The present work was supported by the Austrian Research Promotion Agency (FFG) in the program line “production of the future” under grant number 871438 -project NEAT.

Declaration of Competing Interest

The authors declare that they have no known competing financial interests or personal relationships that could have appeared to influence the work reported in this paper.

Acknowledgements

We would like to thank our project partners: We would like to thank ChanPharm GmbH (Austria) for suggesting the design of the funnel device in Fig. 4 according to DE 102017 130,518 A1 and our project partners PROFACTOR GmbH (Austria) and Institute of Molecular Biotechnology Austria, Stensborg A/S (Denmark).

We thank the Center for Micro- and Nanofabrication (ZMNS) of TU Wien for providing the facility and equipment for microstructure fabrication and characterization.

Appendix A. Supplementary data

Supplementary data to this article can be found online at https://doi.org/10.1016/j.mne.2022.100159.

References

[1] V. Carvalho, et al., 3D printing techniques and their applications to organ-on-a-chip platforms: a systematic review, Sensors 21 (9) (2021) 3304, https://doi.org/10.3390/s21093304.
[2] N. Bhattacharjee, A. Urrios, S. Kang, A. Folch, The upcoming 3D-printing revolution in microfluidics, Lab Chip 16 (10) (2016) 1720–1742, https://doi.org/10.1039/C6LC00163G.
[3] D. Qin, Y. Xia, G.M. Whitesides, Soft lithography for micro- and nanoscale patterning, Nat. Protoc. 5 (3) (2010) 491–502, https://doi.org/10.1038/nprot.2009.234.
[4] R. Šakalys, K.W. Kho, T.E. Keyes, A reproducible, low cost microfluidic microcavity array SERS platform prepared by soft lithography from a 2 photon 3D printed template, Sens. Actuators B Chem. 340 (2021), 129970, https://doi.org/10.1016/j.snb.2021.129970.
[5] J. Shin, et al., Monolithic digital patterning of polydimethylsiloxane with successive laser pyrolysis, Nat. Mater. 20 (1) (2021) 100–107, https://doi.org/10.1038/s41563-020-0769-6.
[6] J. Lim, et al., Monolithic digital patterning of polyimide by laser-induced pyrolytic jetting, Chem. Eng. J. 428 (2022), 131050, https://doi.org/10.1016/j.cej.2021.131050.
[7] S. Waheed, et al., 3D printed microfluidic devices: enablers and barriers, Lab Chip 16 (11) (2016) 1993–2013, https://doi.org/10.1039/C6LC00284F.
[8] C.M.B. Ho, S.H. Ng, K.H.H. Li, Y.-J. Yoon, 3D printed microfluidics for biological applications, Lab Chip 15 (18) (2015) 3627–3637, https://doi.org/10.1039/C5LC00685F.
[9] A.K. Au, W. Huynh, L.F. Horowitz, A. Folch, 3D-printed microfluidics, Angew. Chem. Int. Ed. 55 (12) (2016) 3862–3881, https://doi.org/10.1002/anie.201504382.
[10] V. Mehta, S.N. Rath, 3D printed microfluidic devices: a review focused on four fundamental manufacturing approaches and implications on the field of healthcare, Bio-Des. Manuf. 4 (2) (2021) 311–343, https://doi.org/10.1007/s42242-020-00112-5.
[11] H. Quan, T. Zhang, H. Xu, S. Luo, J. Nie, X. Zhu, Photo-curing 3D printing technique and its challenges, Bioact. Mater. 5 (1) (2020) 110–115, https://doi.org/10.1016/j.bioactmat.2019.12.003.
[12] A.-I. Bunea, N. del Castillo Iniesta, A. Droumpali, A.E. Wetzel, E. Engay, R. Taboryski, Micro 3D printing by two-photon polymerization: configurations and parameters for the nanoscribe system, Micro 1 (2) (2021), https://doi.org/10.3390/micro1020013. Art. no. 2.
[13] S. Kecili, H.C. Tekin, Adhesive bonding strategies to fabricate high-strength and transparent 3D printed microfluidic device, Biomicrofluidics 14 (2) (2020), 024113, https://doi.org/10.1063/5.0003302.
[14] U. Egert, et al., A novel organotypic long-term culture of the rat hippocampus on substrate-integrated multielectrode arrays, Brain Res. Protocol. 2 (4) (1998) 229–242, https://doi.org/10.1016/S1385-299X(98)00013-0.
[15] E. Malishev, et al., Microfluidic device for unidirectional axon growth, J. Phys. Conf. Ser. 643 (2015) 012025, https://doi.org/10.1088/1742-6596/643/1/012025.
[16] D. Kim, H. Kang, Y. Nam, Compact 256-channel multi-well microelectrode array system for in vitro neuropharmacology test, Lab Chip 20 (18) (2020) 3410–3422, https://doi.org/10.1039/D0LC00384K.
[17] J.D. Urbano-Gámez, C. Aracil, F. Perdigones, J.A. Fontanilla, J. Manuel Quero, Towards a 3D-printed and autonomous culture platform integrated with commercial microelectrode arrays’, in: 2021 13th Spanish Conference on Electron Devices (CDE), 2021, pp. 153–155, https://doi.org/10.1109/CDE52135.2021.9455748.
[18] C. Hart, C.M. Didier, F. Sommerhage, S. Rajaraman, Biocompatibility of blank, post-processed and coated 3D printed resin structures with electrogenic cells, Biosensors 10 (11) (2020), https://doi.org/10.3390/bios10110152. Art. no. 11.
[19] J. Barthes, H. Özçelik, M. Hindié, A. Ndreu-Halili, A. Hasan, N.E. Vrana, Cell microenvironment engineering and monitoring for tissue engineering and regenerative medicine: the recent advances, Biomed. Res. Int. 2014 (2014), e921905, https://doi.org/10.1155/2014/921905.
[20] M. Ventre, P.A. Netti, Controlling Cell Functions and Fate with Surfaces and Hydrogels: The Role of Material Features in Cell Adhesion and Signal Transduction, Gels 2 (1) (2016), https://doi.org/10.3390/gels2010012. Art. no. 1.
[21] K.H. Vining, D.J. Mooney, Mechanical forces direct stem cell behaviour in development and regeneration, Nat. Rev. Mol. Cell Biol. 18 (12) (2017) 728–742, https://doi.org/10.1038/nrm.2017.108.
[22] M. Darnell, A. O’Neil, A. Mao, L. Gu, L.L. Rubin, D.J. Mooney, Material microenvironmental properties couple to induce distinct transcriptional programs in mammalian stem cells, Proc. Natl. Acad. Sci. 115 (36) (2018) E8368–E8377, https://doi.org/10.1073/pnas.1802568115.
[23] S.M. Naqvi, L.M. McNamara, Stem cell Mechanobiology and the role of biomaterials in governing mechanotransduction and matrix production for tissue regeneration, Front. Bioeng. Biotechnol. 8 (2020) 1375, https://doi.org/10.3389/fbioe.2020.597661.